Scrutiny of the LiCoO 2 Composite Electrode/Electrolyte Interface by Advanced Electrogravimetry and Implications for Aqueous Li-Ion Batteries

Wanli Gao, Natacha Krins, Christel Laberty-Robert, Hubert Perrot, Ozlem Sel

Scrutiny of the $LiCoO_2$ Composite Electrode/Electrolyte Interface by Advanced Electrogravimetry and Implications for Aqueous Li-ion Batteries

*Wanli Gao[a], Natacha Krins[b], Christel Laberty-Robert[b], Hubert Perrot[a], Ozlem Sel[a,]**

[a] Sorbonne Université, CNRS, Laboratoire Interfaces et Systèmes Electrochimiques, 75005 Paris, France

[b] Sorbonne Université, CNRS, Laboratoire de Chimie de la Matière Condensée de Paris, 75005 Paris, France

Corresponding Author: ozlem.sel@sorbonne-universite.fr

Abstract: Recent tendency in the battery field towards the use of aqueous electrolytes stimulated several studies searching for compatible electrode materials and charge carriers. Still, another aspect to forge ahead is the fundamental understanding of interfacial processes occurring at electrode/electrolyte interface. To this end, we investigated interfacial properties of a model $LiCoO_2$ composite electrode, in Li_2SO_4 aqueous electrolyte through extensively exploiting *operando* Electrochemical Quartz Crystal Microbalance (EQCM) and its coupling with Electrochemical Impedance Spectroscopy (*ac*-electrogravimetry). EQCM revealed a global cation-exchange behavior, which is decoded by *ac*-electrogravimetry into multi-species contribution with different proportions/kinetics, benefited from the capacity of the latter to study interfacial dynamics. Li^+ plays the major role in charge-compensation mechanism but a strong interaction with H_2O has been revealed with close interfacial transfer kinetics, which provides experimental evidence on the essential character of H_2O assisting the Li^+ insertion in

layered materials, due to the weakened charge density by screening the electrostatic interactions between the Li^+ ions and the host lattice of cathode materials.

KEYWORDS: Li-ion batteries, aqueous battery, lithium cobalt oxide, interfacial ion transfer, EQCM, *ac*-electrogravimetry

1. INTRODUCTION

Aqueous Li-ion batteries (Aqu-LIBs) have generated a recent surge of interest since they are constructed with nonflammable, low-cost and environmentally benign water-based electrolytes, offering a highly promising and safe alternative to organic electrolyte-based LIBs.[1-4] The postulated benefits of Aqu-LIBs have stimulated the pursuit for new electrode materials, compatible with narrow electrochemical stability window of aqueous electrolytes.[5] The most widely studied electrode materials in organic LIBs ($LiCoO_2$ (LCO)[6-9] and $LiFePO_4$ (LFP)[10-11] *etc.*) have also been revisited for their potential use in the aqueous analogues.[3] To this end, correlation of the ion insertion behavior in a specific electrolyte and the physico-chemical properties of electrodes are highly beneficial for performance prediction and eventual tuning of the charge storage properties. However, due to the lack of well suitable analytical tools, the understanding of the Li^+ ion transfer behavior in aqueous electrolyte/electrode interface and the estimation of the corresponding transfer kinetics remain challenging. The issues which had been faced in organic electrolytes, whether the solvated Li^+ cations or de-solvated Li^+ cations [12,13] are exchanged during charge storage, also concerns the Aqu-LIBs field. Particularly, the role of free solvent molecules in Li^+ (de)intercalation (from)into electrode materials is of fundamental importance for electrochemical energy storage, which, however, has not been clearly identified since conventional electrochemical techniques can very often only track the charged species transfer.

Therefore, the fundamental studies capable of providing deeper insight into the Li^+ transfer at the electrode/electrolyte interface (EEI) are highly desired. Various methods of characterization have been used for the *ex situ*, *in situ* or *operando* studies of the EEI of batteries.[14-15] These techniques include, but not limited to, the compositional analyses of battery interfaces using X-ray photoelectron spectroscopy

(XPS)[16] and vibrational spectroscopy (Fourier transform infrared spectroscopy (FTIR),[17] Raman spectroscopy[18] and sum frequency generation[19]) and structural analyses of the crystalline phases during (de)lithiation using X-ray diffraction (XRD).[20] Although valuable information related to the structural evolution, redox mechanism, solid-electrolyte interphase (SEI) formation, and side reactions under battery operating conditions can be addressed,[15] these methods are not able to discriminate the ion-solvent co-intercalation process, thoroughly.

As an in-situ coupled electrochemical and piezoelectric probe, electrochemical quartz-crystal microbalance derived methods (EQCM and EQCM with motional resistance or dissipation monitoring) have shown great sensitivity to monitor the mass (gravimetric probe)[21-24], structure (morphological probe)[25-28] and viscoelastic property (mechanical probe)[25-26, 29-30] variation of an electrode during electrochemical processes, allowing the interfacial and ion intercalation phenomena to be explored, both in aqueous and organic electrolytes.

Among the several work reporting the co-intercalation of water, only a few have employed the classical EQCM to study this phenomenon, so that the insertion of Mg^{2+} ions into MnO_2 along with the water molecules, and the partially desolvated Na^+ cation insertion in TiS_2, have been revealed.[31-32] However, specific information regarding cation and H_2O transfer kinetics is still required to refine the definition of "co-intercalation", namely, how and to which extent H_2O molecules accompany the cations.

Targeted at further understanding this ever-controversial but fundamentally important topic, this work exploited the feasibility of a non-classical electrochemical strategy which couples quartz crystal microbalance (QCM) with electrochemical impedance spectroscopy (EIS) (so-called *ac*-electrogravimetry or *ac*-EQCM), which was firstly proposed by Gabrielli *et al.* in 1988.[33] Since then, its

utility in electrochemistry has progressively spread to study different types of conducting polymers and inorganic electroactive materials.[34-35] Benefited from this synergistic coupling,[36-37] the transfer of charged species (such as ions and solvated ions) is measured by electrochemical system via current response (ΔI), and the transfer of non-charged species (such as H_2O) can be detected by the microbalance frequency change (Δf). Furthermore, the interfacial transfer kinetics of both charged and non-charged species can also be determined through frequency-dependent measurements. This coupling expands the capacity of classical EQCM to study interfacial dynamics and it motivates the present work which uses *ac*-electrogravimetry to unravel the charge storage behavior of aqueous battery electrode/electrolyte interface. Here, in this work, EQCM and its EIS coupling are employed to study the flux of species at the interfaces and to scrutinize charge-storage mechanism of composite $LiCoO_2$ electrodes in Li_2SO_4 electrolyte, as a model system for Aqu-LIB EEI.

2. EXPERIMENTAL SECTION

2.1 Sample Preparation. The composite $LiCoO_2$ electrodes were prepared using a typical drop casting method. A suspension was prepared in an agate mortar by mixing $LiCoO_2$ (hydrothermally synthesized according to a protocol previously described,[38] where CoOOH synthesized in a former step was added into 0.5 mol/L LiOH in an autoclave and kept at 170°C for 12 h), poly(vinylidene fluoride)-co-hexafluoropropylene (PVDF-HFP) (Solef® 21508, Solvay Solexis, Italy) and carbon black (Sigma-Aldrich) with a mass ratio of 8:1:1 in N-methylpyrrolidone (NMP) (Sigma-Aldrich) solvent. The resulting suspension was cast on the gold electrode (0.2 cm^2) of the quartz resonator (14 mm in dimeter, gold patterned 9 MHz quartz; AWS, Valencia, Spain) and dried at 80 °C in an oven overnight. A field emission gun scanning electron microscopy (FEG-SEM) (Zeiss, Supra 55) image of the coated quartz resonator is shown in **Figure S1**, indicating a good coverage of the gold electrode deposited on the quartz resonator. A loaded mass of ~ 14 µg was estimated by converting the microbalance frequency change (Δf), in air before and after the casting process, to mass change (Δm) through Sauerbrey equation,[39] i.e., $\Delta f = -C_f \times \Delta m$, where C_f is the experimental sensitivity factor of a 9MHz quartz crystal resonator ($C_f = 16.3\times10^7$ $Hz\cdot g^{-1}\cdot cm^2$).[40]

2.2 Electrochemical Measurements. Before electrochemical measurements, the electrode was cycled 3 times to get a stable cyclic voltammetry (CV) signature in 1 M Li_2SO_4. Then, EQCM and *ac*-electrogravimetry measurements were performed in 1 M Li_2SO_4. The $LiCoO_2$-loaded quartz resonator was used as the working electrode, with Ag/AgCl (3 M KCl saturated with AgCl) and platinum gauze as the reference and counter electrode, respectively. The potential window was confined between 0.6 V and 0.9 V vs. Ag/AgCl in EQCM (the OCV was at ~ 0.16 V vs. Ag/AgCl). The mass change (Δm) of $LiCoO_2$-

loaded electrode on the quartz crystal during electrochemical process can be estimated by the microbalance frequency change (Δf) through Sauerbrey equation, as justified in the **Results and Discussion** and **Figure 1**.

For *ac*-electrogravimetry measurements,[34-35] a four-channel frequency response analyzer (FRA, Solartron 1254) and a lab-made potentiostat (SOTELEM-PGSTAT) were used. The QCM was performed under dynamic regime, and the modified working electrode was polarized at selected potentials to which a sinusoidal small amplitude potential perturbation was superimposed. The frequency range was between 63 KHz and 10 mHz. The mass change, Δm, of the working electrode was measured simultaneously with the *ac* response, ΔI, of the electrochemical system. The experimental electrogravimetric TF ($\Delta m/\Delta E(\omega)$) and the electrochemical TF ($\Delta E/\Delta I(\omega)$) were obtained simultaneously at a given potential and frequency modulation, f (pulsation, $\omega=2\pi f$). The electrochemical TF ($\Delta E/\Delta I(\omega)$) was presented as the charge/potential TF, $\Delta q/\Delta E(\omega)$, which is more convenient to decouple the contribution of charged species. In charge/potential TF, one loop corresponds to one charged species, provided that their kinetics of transfer are adequately different.[36-37]

The electroacoustic admittance measurements were performed using an Agilent 4294A impedance analyzer. The electroacoustic admittance measurements of neat quartz resonator in air and in solution were firstly conducted. After washing with distilled water and subsequent drying, the same quartz resonator was used for deposition of LCO composite electrode. Then, the electroacoustic admittance measurement of composite LCO electrode was performed in air and in solution. The motional resistance

values (ΔR) were obtained from the fitting of the electroacoustic admittance measurements by using Butterworth-Van-Dyke (BVD) model.[41]

3. RESULTS AND DISCUSSION

3.1 Probing LCO/electrolyte interface by gravimetric EQCM. By analogy to a battery material testing, conducting electrodes of the quartz resonator are employed as current collectors and modified with the electrode material of interest (here shown for composite LCO electrodes). This configuration furnishes electrochemical analysis with additional information on quartz resonator characteristics (such as resonant frequency changes (Δf) in response to an electrochemical reaction between the coated layer and the electrolyte).[42] Then, using EQCM as a gravimetric probe,[43] the Δf can be translated into the mass changes of the electrode (Δm) (Sauerbrey interpretation[39]), e.g. Li^+ deinsertion/insertion during charging/discharging of the composite LCO electrode in Li_2SO_4.

However, prior to a gravimetric EQCM analysis, the reliability of correlation between Δf and Δm has to be verified, by evaluating the hydrodynamic[44] and viscoelastic damping effect[45] in the presence of an electrolyte. The linear relationship between the Δf and Δm (or the use of EQCM as a gravimetric probe) is valid for a dense, flat and thin layer rigidly attached on the resonator. In that case, the added layer behaves as an extension of the resonator and follows synchronously its motion without dissipation of energy.

Prior to gravimetric EQCM analyses, it is important to confirm that above mentioned conditions are fulfilled in the specific electrolyte, so that the Δf occurring in response to an electrochemical process is attributed to a true phenomenon. Muramatsu *et al.*[46] proposed a method to easily screen the

experimental conditions (coating characteristics and its interactions with the electrolyte) whether they fall in the gravimetric regime or not. In their approach, the motional resistance change (ΔR_m) (characteristic of the energy dissipation during oscillation) to Δf ratio ($\Delta R_m/\Delta f$ ratio) is conveniently expressed as energy dissipation or viscoelasticity factor of a coating. In the motional resistance to frequency response plot, a reliable region is defined as $\Delta R_m/\Delta f$ ratio $\leq$ 0.01 $\Omega \cdot Hz^{-1}$ for resonators operating at 9 MHz (**Figure 1)**. For a bare resonator, the effect of passage from air to an aqueous electrolyte, which theoretically depends solely on the square root of the density and viscosity of the medium and gives $\Delta R_m/\Delta f$ values of ~ 0.1 $\Omega \cdot Hz^{-1}$.[44] Therefore, the smaller is this ratio, the weaker will be the hydrodynamic effect and the Δf will be exclusively the result of a real mass change.[47] The estimation of the reliability region by Muramatsu *et al.* is based on studying the evolution of $\Delta R_m/\Delta f$ during the cooling-heating cycles of polymer films. The polymer shows lower $\Delta R_m/\Delta f$ ratios at low T (°C), since it is at a more rigid state. With further increase in temperature, the R_m starts to increase without any change in the f. The point where the f starts to change means that the active mass on the resonator starts to change as well, although real mass remains constant. This criterion (for measurements with different loadings on the resonators) is used to estimate the upper limit of the $\Delta R_m/\Delta f$ ratio, *i.e.* $\Delta R_m/\Delta f$ ratio $\leq$ 0.01 $\Omega \cdot Hz^{-1}$ for resonators operating at 9 MHz (where the lower limit is the ideal case, $\Delta R_m/\Delta f$ ratio is equal to 0).

We revisited this approach introduced by Muramatsu *et al.* [46] where the motional resistance change (ΔR_m) (characteristic of the energy dissipation during oscillation) to Δf ratio ($\Delta R_m/\Delta f$) is conveyed as energy dissipation or viscoelasticity factor of the LCO coatings of this study. A reliable region is defined as $\Delta R_m/\Delta f$ ratio $\leq$ 0.01 $\Omega \cdot Hz^{-1}$.[47] **Figure 1** depicts the data evaluating the behavior of a representative LCO

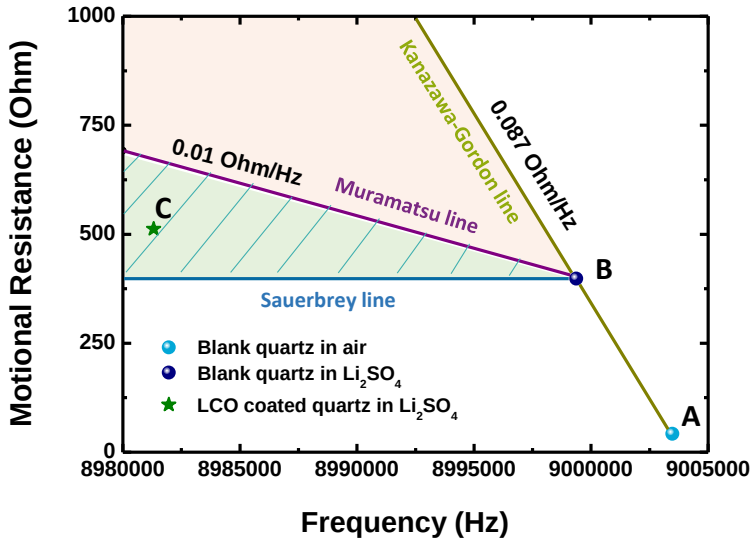

Figure. 1. Resonance frequency (f) versus motional resistance (R_m), for a bare 9MHz quartz resonator in air (A) and in 1M Li_2SO_4 (B), and the same quartz coated with LCO in 1M Li_2SO_4 (C). The dark-yellow line represents the slope of $\Delta R_m/\Delta f$ = 0.087 Ohm/Hz, due to the passage from air to electrolyte, following Kanazawa-Gordon interpretation.[44] The Sauerbrey line[39] (blue) defines the "$\Delta R_m/\Delta f$ =0" extremity and the purple line is the Muramatsu interpretation,[46] defining the upper limit of the gravimetric region with $\Delta R_m/\Delta f$ =0.01 Ohm/Hz.

coated QCM in 1M Li_2SO_4, where its $\Delta R_m/\Delta f$ (point C, **Figure 1**) falls in the gravimetric reliability region between the two extremities of $\Delta R_m/\Delta f$=0 and $\Delta R_m/\Delta f$ =0.01 Ohm/Hz. This finding indicates the validity of using Sauerbrey equation[39] to interpret Δf to Δm for the typical LCO loadings used in this study. After verification, gravimetric EQCM in Li_2SO_4 electrolyte was performed (**Figure 2a**). The composite LCO electrode presents a redox peak at ~ 0.66 V vs. Ag/AgCl, which is commonly attributed to the de(re-)lithiation of Li^+ out of (in) LCO with the reaction: $LiCoO_2 \leftrightarrow Li_{1-x}CoO_2 + xLi^+ + xe^-$.

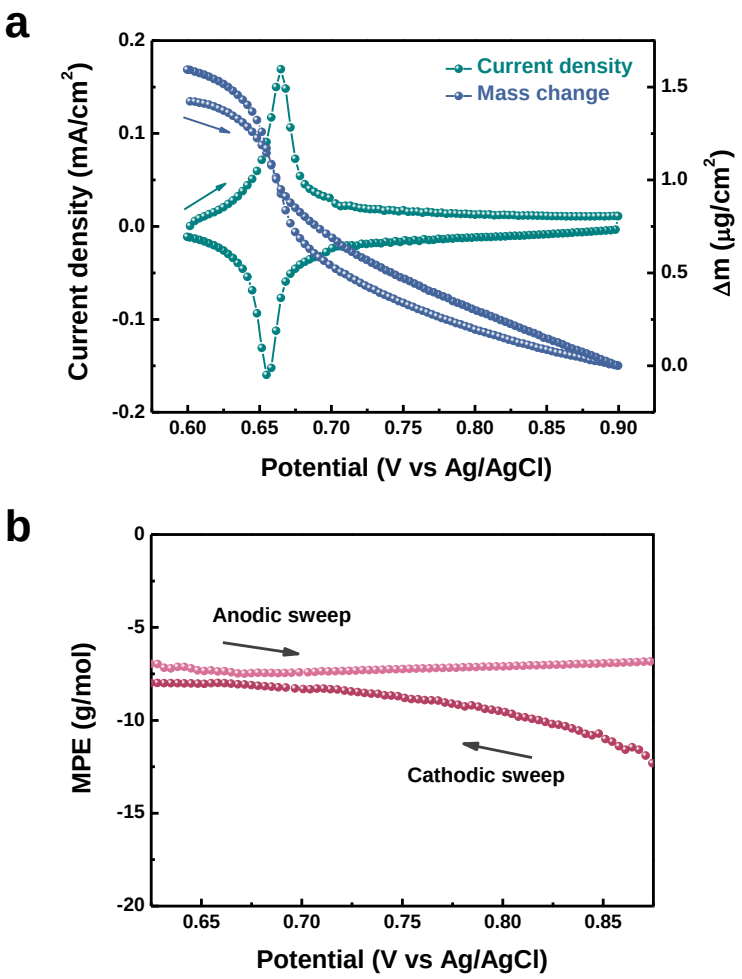

Figure 2. Gravimetric EQCM response (a) and related *MPE* values (b) calculated from panel (a) of composite LCO-coated QCM, in 1 M Li_2SO_4 at a scan rate of 0.5 $mV \cdot s^{-1}$.

Concomitant to this reaction, a mass decrease/increase of ~1.5 $\mu g \cdot cm^{-2}$ is observed during anodic/cathodic sweep (except a slight hysteresis). At a first glance, it is indicative of a major cation-exchange behavior at the EEI and slightly higher mass is exchanged during cathodic sweep. The hysteresis shown in **Figure 2a** (where mass response during anodic and cathodic sweep does not overlap) can be due to the difference between the kinetic rates of the various interfacial transfers related to the insertion/deinsertion of the different species which occur during the charge/discharge process,

respectively. The other observation is that the mass decrease during oxidation is lower than mass increase during reduction (**Figure 2a**). This might indeed mean that there is a mass accumulated on/in the electrode, i.e.; species not to be completely removed from the electrode during the oxidation (delithiation or removal of the solvent molecules) might result in an irreversible mass. To clearly address this point, the cycling behavior of the QCM resonator was inspected (Supporting information file, **Figure S2**). This irreversible mass is estimated to be ~0.033 $\mu g \cdot cm^{-2}$ (thus, negligible over the complete/global mass change ~1.5 $\mu g \cdot cm^{-2}$), after a correction of the QCM frequency over time response (See details in Supporting information file, **Figure S2b**). This non ideal behavior does not affect the *ac*-electrogravimetric measurements (**Part 3.2**), as they were performed under very small potential perturbations.

EQCM data also permits the average mass per mole of electrons ($MPE = F \times (\Delta m/\Delta q)$) to be estimated which provides information on the exchanged species nature during an electrochemical process. Theoretically, if there is only one species participating in charge balance, the absolute *MPE* value would present its molar mass, with negative and positive signs for cations and anions, respectively.[48] **Figure 2b** shows an $|MPE|$ value of ~ 7 $g \cdot mol^{-1}$ above 0.63 V during anodic sweep and ~ 8 $g \cdot mol^{-1}$ below 0.75 V during cathodic sweep. As anticipated, Li^+, with an $|MPE|$ of 7 $g \cdot mol^{-1}$, seems to be the major species exchanged. However, the slight deviation between the experimental and theoretical $|MPE|$ values, especially in cathodic sweep may indicate a multiple-species contribution and complex interfacial behavior (e.g. different flux direction of species may cancel out their contribution), which merits further analysis. To address this issue, frequency-dependent electrogravimetric impedance (*ac*-electrogravimetry) was performed.

3.2 Deconvolution of the species contributions with their transfer kinetics. Apart from the outcome of classical EIS transfer function (TF), $\frac{\Delta E}{\Delta I}(\omega)$, *ac*-electrogravimetry concomitantly provides the mass variation of the electrode in response to a potential perturbation (the so-called mass/potential TF, $\frac{\Delta m}{\Delta E}(\omega)$).[36] Alike EIS, the data is fitted with a suitable model to reach parameters related to the interfacial transfer (kinetics/resistance of transfer and the identification of the species, see fitting details in **Supporting Information File**).

Ac-electrogravimetry was performed at five different states-of-polarization from 0.6 V to 0.9 V vs. Ag/AgCl (**Figure 3** and **Figure S3-S4**). The experimental charge/potential TF ($\frac{\Delta q}{\Delta E}(\omega)$ derived from measured EIS, $\Delta E/\Delta I(\omega)$) ($\frac{\Delta q}{\Delta E}(\omega) = \frac{1}{j\omega}\frac{\Delta I}{\Delta E}(\omega)$) and experimental $\frac{\Delta m}{\Delta E}(\omega)$ were analysed to interpret the charge compensation behavior.[49-51] The $\frac{\Delta q}{\Delta E}(\omega)$ is presented instead of $\frac{\Delta E}{\Delta I}(\omega)$, since the former conveniently decouples the contribution of the charged species transfer (**Figure 3a** and **Figure S3a**).

To estimate the parameters regarding the interfacial transfer properties and nature of the intervening species, the experimental data were fitted using the model described in **Supporting Information File** and the theoretical functions in **equations 1-2**.

$$\frac{\Delta q}{\Delta E}(\omega) = Fd_f \sum_i \frac{G_i}{j\omega d_f + K_i} \qquad (i\text{: ions}) \qquad \textbf{(Equation 1)}$$

$$\frac{\Delta m}{\Delta E}(\omega) = -d_f \sum_i M_i \frac{G_i}{j\omega d_f + K_i} \qquad (i\text{: (non)-ionic species}) \qquad \textbf{(Equation 2)}$$

where K_i represents the interfacial transfer kinetics of each species and G_i quantifies the ease/difficulty of transfer at the coating/electrolyte interface, ω is the pulsation, d_f is the average coating thickness, F is the Faraday constant and M_i depicts involved species molar mass. Unlike $\frac{\Delta q}{\Delta E}(\omega)$, only considering the

ionic species transfer, $\frac{\Delta m}{\Delta E}(\omega)$ also takes non-ionic species transfer into account and identifies the species by their molar masses (M_i). For fitting the experimental data ($\frac{\Delta q}{\Delta E}(\omega)$ and $\frac{\Delta m}{\Delta E}(\omega)$) with the theoretical expressions (**equation 1-2**), several possible configurations involving ionic/non-ionic species in Li_2SO_4 electrolyte were considered. It is revealed that cations (Li^+), H_2O molecules and even anions (SO_4^{2-}) (in)directly participate to charge balance in the potential range studied, with a variation in their quantities and interfacial transfer kinetics. **Figures 3a-b** and **Figure S3** depict two representative analyses at selective potentials of 0.65 V and 0.8 V (close to/far from CV peak potentials in **Figure 2a**, respectively). A good agreement of the experimental/theoretical curves is noted, both in terms of shape and frequencies. Li^+ is exchanged at higher frequencies than H_2O molecules, interestingly SO_4^{2-} is also detected at high frequencies, exhibiting an opposite flux direction to Li^+ and H_2O transfer (**Figure 3a-b**). It is worth mentioning that, SO_4^{2-} contribution is insignificant compared to Li^+ and H_2O during charge balance, but it is not neglected, due to its high molar mass. To ensure this model of $SO_4^{2-}/Li^+/H_2O$ transfer, two partial mass/potential TFs were also analysed (**Figure S4,** details of the cross-check procedure[36] in **Supporting Information File**), which confirms the validity of this configuration (further discussed below).

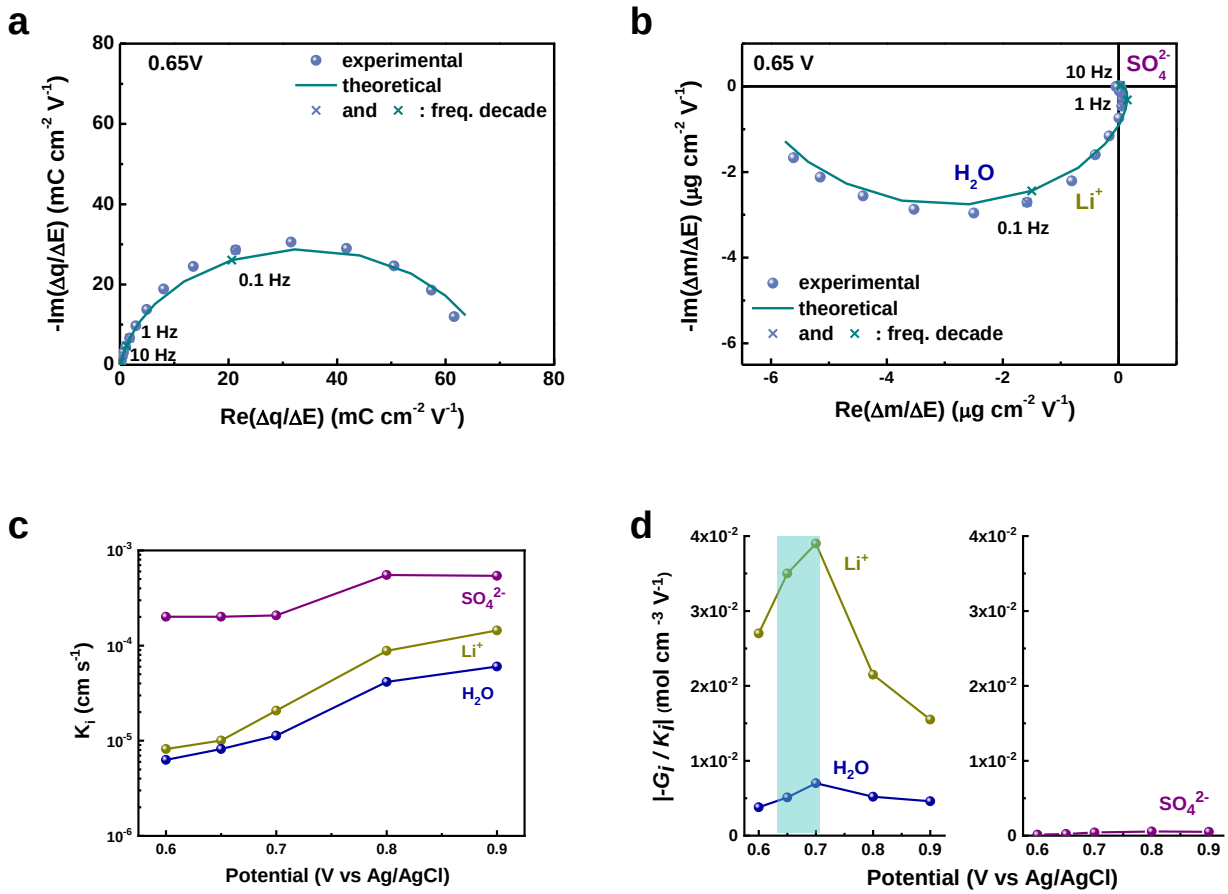

Figure 3. Experimental and theoretical $\Delta q/\Delta E$ (ω) (a) and $\Delta m/\Delta E$ (ω) (b) TFs of the LCO-coated QCM at 0.65 V vs. Ag/AgCl. Panel (c) shows the transfer kinetics, K_i (cm·s^{-1}), as a function of potential and (d) shows the absolute relative concentration changes of each participant with respect to the potential variation (mol·cm^{-3}·V^{-1}) (|-G$_i$/K$_i$|). G_i is the inverse of the transfer resistance (mol·s^{-1}·cm^{-2}·V^{-1}). Note: the marked area in panel (d) is close to the redox peak potential in **Figure 2a**.

As an important asset of *ac*-electrogravimetry, the interfacial transfer kinetics (K_i) of each species can be obtained since these measurements are frequency dependent, *i.e.*, fast/slow species appear at high/low frequency domain of the Nyquist plots, respectively. A similar potential-dependent kinetics of interfacial transfer is found between Li^+ and H_2O (**Figure 3c**), signifying their close interaction while being

transferred. This provides experimental evidence on the essential character of H_2O assisting Li^+ insertion in layered materials, probably due to weakened charge density by screening interlayer electrostatic repulsions. Meanwhile, SO_4^{2-} anions maintain a faster and steadier interfacial kinetics compared with Li^+ and H_2O throughout the overall potential window, which is likely ascribed to their fast surface-controlled transfer.[52] The possible electroadsorption sites for SO_4^{2-} are carbon black (composite electrode contains 10 wt%) and gold substrate surface (despite being modified with a homogeneous coating, electrolyte may have access to gold substrate, sulfates are known for their affinity to the latter[53]). The possibility of SO_4^{2-} intercalation is discarded due to its size (diameter is 0.484 nm, larger than d-spacing of LCO, 0.47nm).[54]

Figure 3d further compares the absolute relative concentration changes of each species with respect to the potential variation at different polarization states by calculating $|-G_i/K_i|$ ($mol \cdot cm^{-3} \cdot V^{-1}$) (details are given in following section of the results and discussion **3.3** and **equation 3**). Consistently, Li^+ and H_2O present a synchronous behavior change, with $|-G_i/K_i|$ peaking around CV redox peak potentials (at about 0.6-0.7 V vs. Ag/AgCl where the intercalation of Li^+ occurs). This is a strong experimental support for the co-intercalation of H_2O and, to the best of our knowledge, cannot be reached by other characterization methods of the electrode/electrolyte interfaces. Regarding the anion contribution, the $|-G_i/K_i|$ of SO_4^{2-} presents a significantly smaller value compared to that of Li^+ and H_2O, and roughly increases towards positive potential range. This implies that very small quantities of SO_4^{2-} anions are favorably transferred at positive potential range, which proves their aforementioned electroadsorption character.

Turning to Li^+ and considering its hydration number which can reach as high as 22 ($Li^+.nH_2O$, n=22) in bulk electrolyte,[55] Li^+ should get rid of its thick H_2O sheath upon insertion into LCO lattice. Thus, Li^+ transfer at the EEI is slower compared to the transfer of anions which is presumably driven by an

electroadsorption process, as argumented earlier (**Figure 3c**). Though bare Li^+ is found to be transferred at the EEI and compensate the redox of LCO (**Figure 3**), a strong interaction between Li^+ and H_2O has been revealed by *ac*-electrogravimetry (close transfer kinetics in **Figure 3c**). It is noted that LCO is a layered material with *d-spacing* of ~0.47nm,[3, 56] larger than the diameter of H_2O molecules (~0.274nm),[57-58] making it possible for H_2O to participate to Li^+ intercalation process.

To verify the findings of *ac*-electrogravimetry, which separated global mass variation of EQCM (**Figure 2a**) into distinct contributions of SO_4^{2-}, Li^+ and H_2O; a verification procedure based on the complementarity of the two techniques has been applied, as described below.

3.3 Complementarity of EQCM and *ac*-electrogravimetry. The relative concentration changes of each participant (ΔC_i) with respect to the potential variation (ΔE) can be estimated from *ac*-electrogravimetry by considering the low frequency limit of the concentration/potential TF, (**equation 3**).

$$\frac{\Delta C_i}{\Delta E}(\omega) = \frac{-G_i}{j\omega d_f + K_i} \qquad (\text{for } \omega \to 0) \qquad \frac{\Delta C_i}{\Delta E}(\omega) = \frac{-G_i}{K_i} \qquad \textbf{(Equation 3)}$$

After integration of **equation 3** with respect to potential, the relative concentration changes of each participant between different states-of-polarization (C_i - C_0) can be estimated as shown in **equation 4**:

$$C_i - C_0 = \int_{E_0}^{E_i} \frac{\Delta C_i}{\Delta E}(\omega)\, dE \Big|_{\omega \to 0} = \int_{E_0}^{E_i} \frac{-G_i}{K_i}\, dE \qquad \textbf{(Equation 4)}$$

Figure 4a displays the relative concentration changes (C_i - C_0) of individual species identified from *ac*-electrogravimetry. Li^+ presents the highest concentration change in the potential range from 0.9 V to 0.6 V vs. Ag/AgCl, followed by the H_2O concentration change with the same flux direction. Contrarily, SO_4^{2-} anions exhibit an opposite flux direction relative to Li^+ with only slight increase of relative

concentration changes in the applied potential range, corresponding to the very small response in $\frac{\Delta m}{\Delta E}(\omega)$ (**Figure 3b**). This result confirms the major role of Li^+ in charge-storage mechanism of LCO in aqueous electrolytes (ΔC of SO_4^{2-} is significantly smaller).

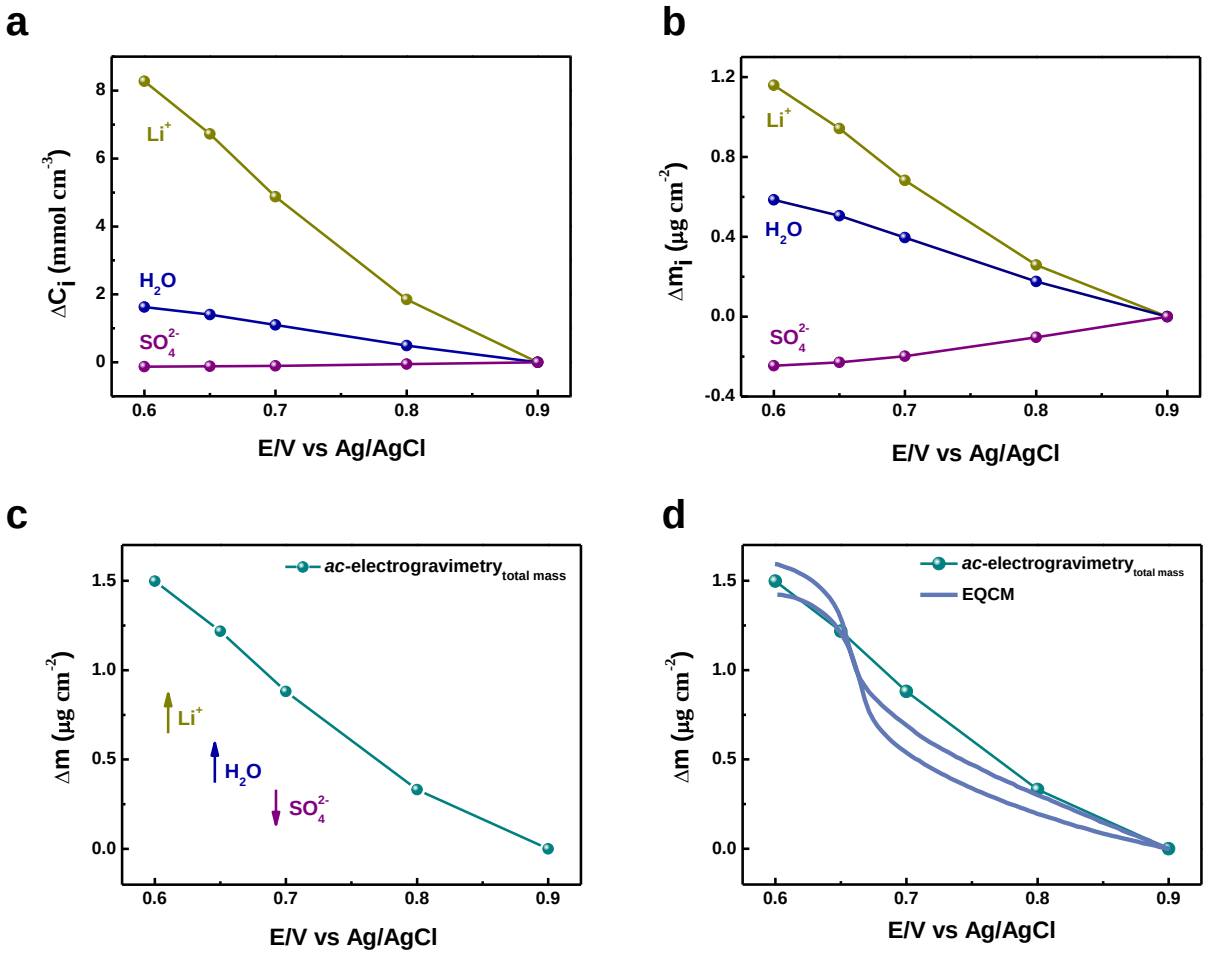

Figure 4. Relative concentration changes (a) and corresponding mass changes (b) of each species as a function of potential, Δm re-constructed from *ac*-electrogravimetry (c) and the comparison of Δm obtained from EQCM (at 0.5 $mV \cdot s^{-1}$) and *ac*-electrogravimetry (d). Arrows in panel c indicate the flux directions of species during a cathodic sweep.

The relative concentration changes (C_i - C_0) of each participant can be turned into corresponding mass

variations (**Figure 4b**) with consideration of their molar masses (M_i). By the addition of individual mass contributions from all participants identified in *ac*-electrogravimetry, the total gravimetric response can be recalculated (**Figure 4c**), which presents a perfect match with the mass change measured in EQCM (**Figure 4d**). This verification step ensures the multi-species exchange in charge-storage mechanism of the present system, and highlights the significant contribution of H_2O molecules along with Li^+ transfer (**Figure 4a** and **4b**).

4. CONCLUSIONS

In conclusion, we have examined the EEI behavior of a model composite LCO electrode in Li_2SO_4 by advanced electrogravimetry, motivated by increasing interest in Aqu-LIBs in energy community. Classical gravimetric EQCM revealed a global cation-exchange behavior which is decoded into a multi-species contribution (SO_4^{2-}, Li^+ and H_2O) with different proportions and kinetics, by frequency-dependent *ac*-electrogravimetry. A strong interaction between Li^+ and H_2O has been detected, as indicated by their close transfer kinetics. Furthermore, for both Li^+ and H_2O, the absolute relative concentration changes of with respect to the potential variation ($mol \cdot cm^{-3} \cdot V^{-1}$), ($\Delta C_i/\Delta E$, equivalent to $|-G_i/K_i|$) reach a peak point between 0.6-0.7 V vs. Ag/AgCl, where the intercalation of Li^+ occurs, which is a strong experimental support for the co-intercalation of H_2O. Indeed, water assisted cation intercalation concept dates back 1993, where Novak *et al.* revealed the facilitating effect of water on Mg^{2+} during intercalation process in V_2O_5 and MoO_3.[59-60] This concept has been revisited in recent studies, parallel with the growing interest towards aqueous batteries (Li^+, Na^+ and Mg^{2+} intercalation in prussian blue analogs,[61-62] Mg^{2+} in MnO_2,[31] Zn^{2+} in $V_3O_7.H_2O$,[63] Na^+ in TiS_2[32]) where it is postulated

that the water molecules facilitate the insertion of the charge carrier in the material. Our results provided by EQCM and *ac*-electrogravimetry bolster these previous observations, by providing experimental evidence. Further studies will focus on electrolyte composition (different concentrations and pH) to study the effect of possible H^+ intercalation preference over Li^+ insertion (H^+ may covalently bond to oxygen atoms of LCO, blocking the channels for Li^+ diffusion, degrading cycling performance[64]). The methodology can also be extended to study other EEI which can contribute to the development of Aqu-LIBs, as well as newly emerging counterparts using multivalent ions as charge carriers.

ASSOCIATED CONTENT

Morphological characterization, details of the EQCM analyses, additional *ac*-electrogravimetry results of composite $LiCoO_2$ electrodes, as well as the model used for fitting the *ac*-electrogravimetry data and partial TFs indicating the validity of the model.

AUTHOR INFORMATION

Corresponding author: ozlem.sel@sorbonne-universite.fr

Notes

The authors declare no competing financial interests.

ACKNOWLEDGMENT

This work was supported by the ANR under reference ANR-11-IDEX-0004-02 and by the Cluster of Excellence LABEX MATISSE led by Sorbonne Université.

REFERENCES

1. W. Li; J. R. Dahn; Wainwright, D. S., Rechargeable Lithium Batteries with Aqueous Electrolytes. *Science* **1994**, *264*, 1115.
2. Xue, L.; Zhang, Q.; Zhu, X.; Gu, L.; Yue, J.; Xia, Q.; Xing, T.; Chen, T.; Yao, Y.; Xia, H., 3d $LiCoO_2$ Nanosheets Assembled Nanorod Arrays Via Confined Dissolution-Recrystallization for Advanced Aqueous Lithium-Ion Batteries. *Nano Energy* **2019**, *56*, 463-472.
3. Ramanujapuram, A.; Gordon, D.; Magasinski, A.; Ward, B.; Nitta, N.; Huang, C.; Yushin, G., Degradation and Stabilization of Lithium Cobalt Oxide in Aqueous Electrolytes. *Energy Environ. Sci.* **2016**, *9*, 1841-1848.
4. Demir-Cakan, R.; Palacin, M. R.; Croguennec, L., Rechargeable Aqueous Electrolyte Batteries: From Univalent to Multivalent Cation Chemistry. *J. Mater. Chem. A* **2019**, *7*, 20519-20539.
5. Chao, D.; Zhou, W.; Xie, F.; Ye, C.; Li, H.; Jaroniec, M.; Qiao, S.-Z., Roadmap for Advanced Aqueous Batteries. *Sci. Adv.* **2020**, *6*, eaba4098.
6. Wang, L.; Chen, B.; Ma, J.; Cui, G.; Chen, L., Reviving Lithium Cobalt Oxide-Based Lithium Secondary Batteries-toward a Higher Energy Density. *Chem. Soc. Rev.* **2018**, *47*, 6505-6602.
7. Xie, J.; Zhao, J.; Liu, Y.; Wang, H.; Liu, C.; Wu, T.; Hsu, P.-C.; Lin, D.; Jin, Y.; Cui, Y., Engineering the Surface of $LiCoO_2$ Electrodes Using Atomic Layer Deposition for Stable High-Voltage Lithium Ion Batteries. *Nano Res.* **2017**, *10*, 3754-3764.
8. Tarascon, J. M.; Armand, M., Issues and Challenges Facing Rechargeable Lithium Batteries. *Nature* **2001**, *414*, 359-367.
9. Duffiet, M.; Blangero, M.; Cabelguen, P. E.; Delmas, C.; Carlier, D., Influence of the Initial Li/Co Ratio in $LiCoO_2$ on the High-Voltage Phase-Transitions Mechanisms. *J. Phys. Chem. Lett.* **2018**, *9*, 5334-5338.
10. Gibot, P.; Casas-Cabanas, M.; Laffont, L.; Levasseur, S.; Carlach, P.; Hamelet, S.; Tarascon, J. M.; Masquelier, C., Room-Temperature Single-Phase Li Insertion/Extraction in Nanoscale Li_xFePO_4. *Nat. Mater.* **2008**, *7*, 741-747.
11. Koltypin, M.; Aurbach, D.; Nazar, L.; Ellis, B., On the Stability of $LiFePO_4$ Olivine Cathodes under Various Conditions (Electrolyte Solutions, Temperatures). *Electrochem. Solid State Lett.* **2007**, *10*, A40-A44.
12. Fu, L. J.; Liu, H.; Li, C.; Wu, Y. P.; Rahm, E.; Holze, R.; Wu, H. Q., Surface Modifications of Electrode Materials for Lithium Ion Batteries. *Solid State Sci.* **2006**, *8*, 113-128.
13. Jow, T. R.; Delp, S. A.; Allen, J. L.; Jones, J.-P.; Smart, M. C., Factors Limiting Li^+ Charge Transfer Kinetics in Li-Ion Batteries. *J. Electrochem. Soc.* **2018**, *165*, A361-A367.
14. Tripathi, A. M.; Su, W.-N.; Hwang, B. J., In Situ Analytical Techniques for Battery Interface Analysis. *Chem. Soc. Rev.* **2018**, *47*, 736-851.
15. Liu, D., et al., Review of Recent Development of in Situ/Operando Characterization Techniques for Lithium Battery Research. *Adv. Mater.* **2019**, *31*, 1806620.
16. Schulz, N.; Hausbrand, R.; Dimesso, L.; Jaegermann, W., XPS-Surface Analysis of SEI Layers on Li-Ion Cathodes: Part I. Investigation of Initial Surface Chemistry. *J. Electrochem. Soc.* **2018**, *165*, A819-A832.
17. Zhang, Y., et al., Revealing Electrolyte Oxidation Via Carbonate Dehydrogenation on Ni-Based Oxides in Li-Ion Batteries by in Situ Fourier Transform Infrared Spectroscopy. *Energy Environ. Sci.* **2020**, *13*, 183-199.
18. Wei, Z.; Salehi, A.; Lin, G.; Hu, J.; Jin, X.; Agar, E.; Liu, F., Probing Li-Ion Concentration in an Operating Lithium Ion Battery Using in Situ Raman Spectroscopy. *J. Power Sources* **2020**, *449*, 227361.
19. Nicolau, B. G.; García-Rey, N.; Dryzhakov, B.; Dlott, D. D., Interfacial Processes of a Model Lithium Ion Battery Anode

Observed, in Situ, with Vibrational Sum-Frequency Generation Spectroscopy. *J. Phys. Chem. C* **2015**, *119*, 10227-10233.

20. Bock, D. C.; Pelliccione, C. J.; Zhang, W.; Timoshenko, J.; Knehr, K. W.; West, A. C.; Wang, F.; Li, Y.; Frenkel, A. I.; Takeuchi, E. S.; Takeuchi, K. J.; Marschilok, A. C., Size Dependent Behavior of Fe_3O_4 Crystals During Electrochemical (De)Lithiation: An in Situ X-Ray Diffraction, Ex Situ X-Ray Absorption Spectroscopy, Transmission Electron Microscopy and Theoretical Investigation. *Phys. Chem. Chem. Phys.* **2017**, *19*, 20867-20880.

21. Sevinc, S.; Tekin, B.; Ata, A.; Morcrette, M.; Perrot, H.; Sel, O.; Demir-Cakan, R., In-Situ Tracking of $NaFePO_4$ Formation in Aqueous Electrolytes and Its Electrochemical Performances in Na-Ion/Polysulfide Batteries. *J. Power Sources* **2019**, *412*, 55-62.

22. Levi, M. D.; Sigalov, S.; Salitra, G.; Elazari, R.; Aurbach, D.; Daikhin, L.; Presser, V., In Situ Tracking of Ion Insertion in Iron Phosphate Olivine Electrodes Via Electrochemical Quartz Crystal Admittance. *J. Phys. Chem. C* **2013**, *117*, 1247-1256.

23. Song, X.; Liu, T.; Amine, J.; Duan, Y.; Zheng, J.; Lin, Y.; Pan, F., In-Situ Mass-Electrochemical Study of Surface Redox Potential and Interfacial Chemical Reactions of Li(Na)$FePO_4$ Nanocrystals for Li(Na)-Ion Batteries. *Nano Energy* **2017**, *37*, 90-97.

24. Lemaire, P.; Dargon, T.; Alves Dalla Corte, D.; Sel, O.; Perrot, H.; Tarascon, J. M., Making Advanced Electrogravimetry as an Affordable Analytical Tool for Battery Interface Characterization. *Anal. Chem.* **2020**, *92*, 13803−13812.

25. Shpigel, N.; Levi, M. D.; Sigalov, S.; Daikhin, L.; Aurbach, D., In Situ Real-Time Mechanical and Morphological Characterization of Electrodes for Electrochemical Energy Storage and Conversion by Electrochemical Quartz Crystal Microbalance with Dissipation Monitoring. *Acc. Chem. Res.* **2018**, *51*, 69-79.

26. Shpigel, N.; Levi, M. D.; Aurbach, D., EQCM-D Technique for Complex Mechanical Characterization of Energy Storage Electrodes: Background and Practical Guide. *Energy Storage Mater.* **2019**, *21*, 399-413.

27. Shpigel, N., et al., In Situ Hydrodynamic Spectroscopy for Structure Characterization of Porous Energy Storage electrodes. *Nat. Mater.* **2016**, *15*, 570-575.

28. Levi, M. D.; Shpigel, N.; Sigalov, S.; Dargel, V.; Daikhin, L.; Aurbach, D., In Situ Porous Structure Characterization of Electrodes for Energy Storage and Conversion by EQCM-D: A Review. *Electrochim. Acta* **2017**, *232*, 271-284.

29. Shpigel, N.; Levi, M. D.; Cheng, X.; Cao, T.; Wu, R.; Mathis, T. S.; Zhang, Y.; Aurbach, D.; Gogotsi, Y., Diffusion-Induced Transient Stresses in Li-Battery Electrodes Imaged by Electrochemical Quartz Crystal Microbalance with Dissipation Monitoring and Environmental Scanning Electron Microscopy. *ACS Energy Lett.* **2019**, *4*, 1907-1917.

30. Kitz, P. G.; Lacey, M. J.; Novak, P.; Berg, E. J., Operando EQCM-D with Simultaneous in Situ Eis: New Insights into Interphase Formation in Li Ion Batteries. *Anal. Chem.* **2019**, *91*, 2296-2303.

31. Song, J.; Noked, M.; Gillette, E.; Duay, J.; Rubloff, G.; Lee, S. B., Activation of a MnO_2 Cathode by Water-Stimulated Mg^{2+} Insertion for a Magnesium Ion Battery. *Phys. Chem. Chem. Phys.* **2015**, *17*, 5256-5264.

32. Srimuk, P.; Lee, J.; Budak, O.; Choi, J.; Chen, M.; Feng, G.; Prehal, C.; Presser, V., In Situ Tracking of Partial Sodium Desolvation of Materials with Capacitive, Pseudocapacitive, and Battery-Like Charge/Discharge Behavior in Aqueous Electrolytes. *Langmuir* **2018**, *34*, 13132-13143.

33. Bourkane, S.; Gabrielli, C.; Keddam, M., Kinetic Study of Electrode Processes by Ac Quartz Electrogravimetry. *J. Electroanal. Chem.* **1988**, *256*, 471-475.

34. Gabrielli, C.; Garcia-Jareno, J. J.; Keddam, M.; Perrot, H.; Vicente, F., Ac-Electrogravimetry Study of Electroactive Thin Films. I. Application to Prussian Blue. *J. Phys. Chem. B* **2002**, *106*, 3182-3191.

35. Gabrielli, C.; Garcia-Jareno, J. J.; Keddam, M.; Perrot, H.; Vicente, F., Ac-Electrogravimetry Study of Electroactive Thin Films. Ii. Application to Polypyrrole. *J. Phys. Chem. B* **2002**, *106*, 3192-3201.

36. Arias, C. R.; Debiemme-Chouvy, C.; Gabrielli, C.; Laberty-Robert, C.; Pailleret, A.; Perrot, H.; Sel, O., New Insights into Pseudocapacitive Charge-Storage Mechanisms in Li-Birnessite Type MnO_2 Monitored by Fast Quartz Crystal Microbalance Methods. *J. Phys. Chem. C* **2014**, *118*, 26551-26559.

37. Lemaire, P.; Sel, O.; Alves Dalla Corte, D.; Iadecola, A.; Perrot, H.; Tarascon, J.-M., Elucidating the Origin of the Electrochemical Capacity in a Proton-Based Battery H_xIrO_4 Via Advanced Electrogravimetry. *ACS Appl. Mater. Interfaces* **2020**, *12*, 4510-4519.

38. Rano, S.; Laberty-Robert, C.; Ngo, K.; Sanchez-Sanchez, C. M.; Vivier, V., Characterization of $LiCoO_2$ Nanoparticle Suspensions by Single Collision Events. *Phys. Chem. Chem. Phys.* **2019**, *21*, 5416-5423.

39. Sauerbrey, G., Verwendung Von Schwingquarzen Zur Wägung Dünner Schichten Und Zur Mikrowägung. *Zeitschrift für physik* **1959**, *155*, 206-222.

40. Bizet, K.; Gabrielli, C.; Perrot, H., Immunodetection by Quartz Crystal Microbalance. *Appl. Biochem. Biotechnol.* **2000**, *89*, 139-149.

41. John, J.; Hugar, K. M.; Rivera-Melendez, J.; Kostalik, H. A. t.; Rus, E. D.; Wang, H.; Coates, G. W.; Abruna, H. D., An Electrochemical Quartz Crystal Microbalance Study of a Prospective Alkaline Anion Exchange Membrane Material for Fuel Cells: Anion Exchange Dynamics and Membrane Swelling. *J. Am. Chem. Soc.* **2014**, *136*, 5309-5322.

42. Levi, M. D.; Salitra, G.; Levy, N.; Aurbach, D.; Maier, J., Application of a Quartz-Crystal Microbalance to Measure Ionic Fluxes in Microporous Carbons for Energy Storage. *Nat. Mater.* **2009**, *8*, 872-875.

43. Hillman, A. R., The Eqcm: Electrogravimetry with a Light Touch. *J. Solid State Electrochem.* **2011**, *15*, 1647-1660.

44. Keiji Kanazawa, K.; Gordon, J. G., The Oscillation Frequency of a Quartz Resonator in Contact with Liquid. *Anal. Chim. Acta* **1985**, *175*, 99-105.

45. Johannsmann, D., Viscoelastic, Mechanical, and Dielectric Measurements on Complex Samples with the Quartz Crystal Microbalance. *Phys. Chem. Chem. Phys.* **2008**, *10*, 4516-4534.

46. Muramatsu, H.; Egawa, A.; Ataka, T., Reliability of Correlation between Mass Change and Resonant Frequency Change for a Viscoelastic-Film-Coated Quartz Crystal. *J. Electroanal. Chem.* **1995**, *388*, 89-92.

47. Agrisuelas, J.; Gabrielli, C.; García-Jareño, J. J.; Perrot, H.; Sel, O.; Vicente, F., Viscoelastic Potential-Induced Changes in Acoustically Thin Films Explored by Quartz Crystal Microbalance with Motional Resistance Monitoring. *Electrochim. Acta* **2015**, *176*, 1454-1463.

48. Bruckenstein, S.; Jureviciute, I.; Hillman, A. R., Use of the Flux Ratio Method for Mechanistic Diagnosis in Electroactive Polymer Film Redox Switching. *J. Electrochem. Soc.* **2003**, *150*, E285-E291.

49. Gao, W.; Demir-Cakan, R.; Perrot, H.; Sel, O., Electrochemically Reduced Graphene Oxide-Sheltered ZnO Nanostructures Showing Enhanced Electrochemical Performance Revealed by an in Situ Electrogravimetric Study. *Adv. Mater. Interfaces* **2019**, *6*, 1801855.

50. Gao, W.; Perrot, H.; Sel, O., Tracking Interfacial Charge Transfer Behavior of Hydrothermally Synthesized ZnO Nanostructures Via Complementary Electrogravimetric Methods. *Phys. Chem. Chem. Phys.* **2018**, *20*, 27140-27148.

51. Escobar-Teran, F.; Arnau, A.; Garcia, J. V.; Jiménez, Y.; Perrot, H.; Sel, O., Gravimetric and Dynamic Deconvolution of Global Eqcm Response of Carbon Nanotube Based Electrodes by Ac-Electrogravimetry. *Electrochem. Commun.* **2016**, *70*, 73-77.

52. Li, H.-H.; Zhou, L.; Zhang, L.-L.; Fan, C.-Y.; Fan, H.-H.; Wu, X.-L.; Sun, H.-Z.; Zhang, J.-P., Co_3O_4 Nanospheres Embedded in a Nitrogen-Doped Carbon Framework: An Electrode with Fast Surface-Controlled Redox Kinetics for Lithium Storage. *ACS Energy Lett.* **2017**, *2*, 52-59.

53. Kasuya, M.; Sogawa, T.; Masuda, T.; Kamijo, T.; Uosaki, K.; Kurihara, K., Anion Adsorption on Gold Electrodes

Studied by Electrochemical Surface Forces Measurement. *J. Phys. Chem. C* **2016**, *120*, 15986-15992.

54. Marcus, Y., Ionic Radii in Aqueous Solutions. *Chem. Rev.* **1988**, *88*, 1475−1498.

55. Levi, M. D.; Sigalov, S.; Salitra, G.; Elazari, R.; Aurbach, D., Assessing the Solvation Numbers of Electrolytic Ions Confined in Carbon Nanopores under Dynamic Charging Conditions. *J. Phys. Chem. Lett.* **2011**, *2*, 120-4.

56. Shao-Horn, Y.; Croguennec, L.; Delmas, C.; Nelson, E. C.; O'Keefe, M. A., Atomic Resolution of Lithium Ions in $LiCoO_2$. *Nat. Mater.* **2003**, *2*, 464-467.

57. Schatzberg, P., On the Molecular Diameter of Water from Solubility and Diffusion Measurements. *J. Phys. Chem.* **1967**, *71*, 4569-4570.

58. Zhang, Y.; Xu, Z., Atomic Radii of Noble Gas Elements in Condensed Phases. *Am. Mineral.* **1995**, *80* 670−675.

59. Novák, P., Electrochemical Insertion of Magnesium in Metal Oxides and Sulfides from Aprotic Electrolytes. *J. Electrochem. Soc.* **1993**, *140*, 140-144.

60. Guduru, R. K.; Icaza, J. C., A Brief Review on Multivalent Intercalation Batteries with Aqueous Electrolytes. *Nanomaterials* **2016**, *6*.

61. Mizuno, Y.; Okubo, M.; Hosono, E.; Kudo, T.; Zhou, H.; Oh-ishi, K., Suppressed Activation Energy for Interfacial Charge Transfer of a Prussian Blue Analog Thin Film Electrode with Hydrated Ions (Li^+, Na^+, and Mg^{2+}). *J. Phys. Chem. C* **2013**, *117*, 10877-10882.

62. Chen, L.; Shao, H.; Zhou, X.; Liu, G.; Jiang, J.; Liu, Z., Water-Mediated Cation Intercalation of Open-Framework Indium Hexacyanoferrate with High Voltage and Fast Kinetics. *Nat. Commun.* **2016**, *7*, 11982.

63. Kundu, D.; Hosseini Vajargah, S.; Wan, L.; Adams, B.; Prendergast, D.; Nazar, L. F., Aqueous Vs. Nonaqueous Zn-Ion Batteries: Consequences of the Desolvation Penalty at the Interface. *Energy Environ. Sci.* **2018**, *11*, 881-892.

64. Gu, X.; Liu, J.; Yang, J.; Xiang, H.; Gong, X.; Xia, Y. First-Principles Study of H^+ Intercalation in Layer-Structured $LiCoO_2$. *J. Phys. Chem. C* **2011**, 115, 12672−12676

TOC

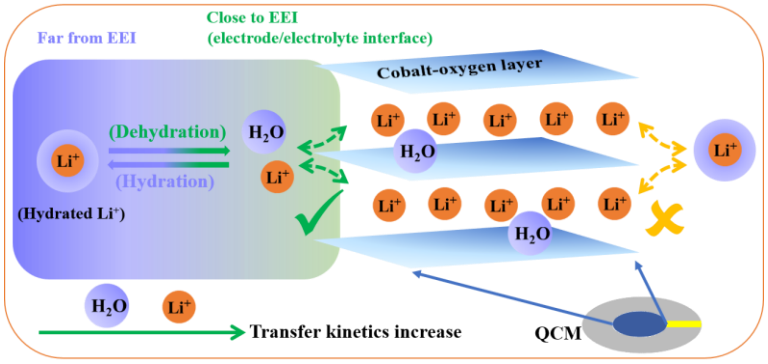
Far from EEI
Close to EEI
(electrode/electrolyte interface)
Cobalt-oxygen layer
(Dehydration)
(Hydration)
(Hydrated Li+)
Transfer kinetics increase
QCM